Robotics Research Technical Report

A Miniature Pan-Tilt Actuator: the Spherical Pointing Motor

by

Benjamin Bederson, Richard Wallace and Eric Schwartz

Technical Report No. 601
Robotics Report No. 264
March, 1992

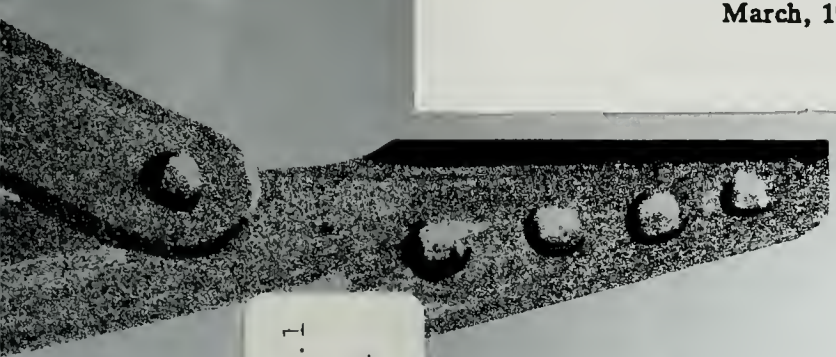

NYU COMPSCI TR-601
Bederson, Benjamin c.1
A miniature pan-tilt
actuator: the spherical
pointing motor.

Courant Institute of Mathematical Sciences
New York University
Computer Science Division
715 Broadway, 12th floor New York, N.Y. 10012

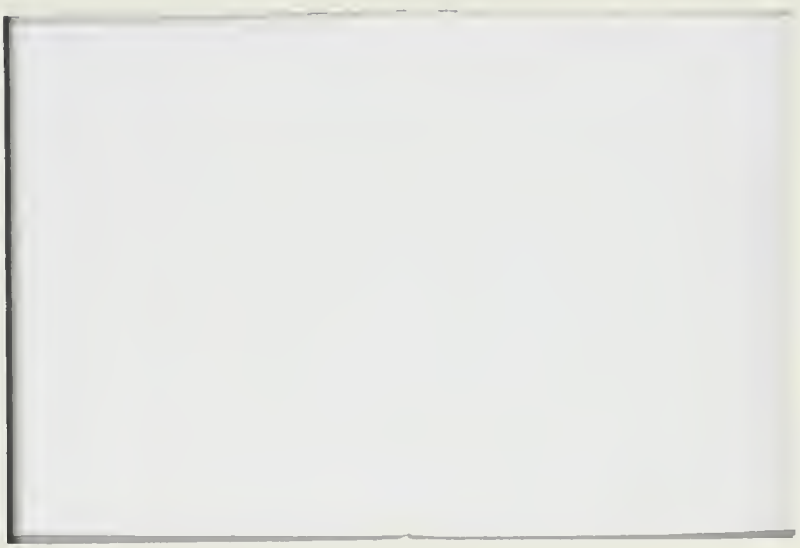

A Miniature Pan-Tilt Actuator: the Spherical Pointing Motor

by

Benjamin Bederson, Richard Wallace
and Eric Schwartz

Technical Report No. 601
Robotics Report No. 264
March, 1992

New York University
Dept. of Computer Science
Courant Institute of Mathematical Sciences
251 Mercer Street
New York, New York 10012

Work on this paper has been supported by DARPA/ONR grant #N00014-90-C-0049,and AFOSR grant #88-0275.

A Miniature Pan-Tilt Actuator: the Spherical Pointing Motor *

Benjamin B. Bederson †‡
Richard S. Wallace ‡
Eric L. Schwartz †‡§

†Courant Institute of Mathematical Sciences
New York University
251 Mercer Street
New York, NY 10012

‡Vision Applications, Inc.
611 Broadway #714
New York, NY 10012

§Computational Neuroscience Laboratory
Department of Psychiatry
New York University Medical Center
550 First Avenue
New York, NY 10016

April 7, 1992

Abstract

A pan-tilt mechanism is a computer-controlled actuator designed to point an object such as a camera sensor. For applications in active vision, a pan-tilt mechanism should be accurate, fast, small, inexpensive and have low power requirements. We have designed and constructed a new type of actuator meeting these requirements , which incorporates both pan and tilt into a single, two degree of freedom device. The Spherical Pointing Motor (SPM) consists of three orthogonal motor windings in a permanent magnetic field, configured to move a small camera mounted on a gimbal. It is an absolute positioning device and is run open loop. The SPM is capable of panning and tilting a load of 15 grams, for example a CCD image sensor, at rotational velocities of several hundred degrees per second with an accuracy of .15°. We have also built a miniature camera consisting of a single CCD sensor chip and miniature lens assembly that fits on the rotor of this motor. In this paper, we discuss the theory of the SPM which includes its basic electromagnetic principles and derive the relationship between applied currents and resultant motor position. We present an

*This work supported in part by DARPA/ONR Contract #N00014-90-C-0049, and AFOSR Contract #88-0275. Please direct all correspondence to the authors at Vision Applications, Inc., 611 Broadway #714, New York, NY 10012

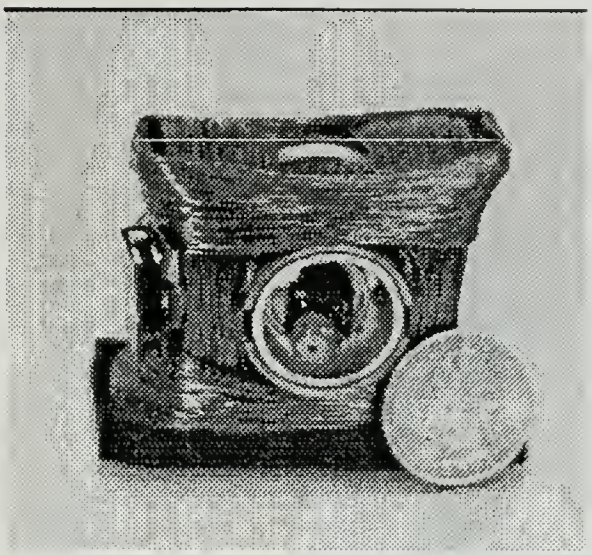

Figure 1: The Spherical Pointing Motor. At the center is a miniature camera consisting of a single CCD sensor chip and a lens assembly that fits on the rotor.

automatic calibration procedure and discuss open and closed-loop control strategies. Finally, we present the physical characteristics and results of our prototype.

1 Introduction

A pan-tilt mechanism is a computer-controlled actuator designed to point an object such as a camera sensor. For applications in active vision, it is desirable for a pan-tilt mechanism to be accurate, fast, small, inexpensive and to have low power requirements. We have constructed a new type of actuator meeting these requirements. It incorporates both pan and tilt into a single two degree of freedom device (Figure 1). The Spherical Pointing Motor (SPM) consists of three orthogonal motor windings in a permanent magnetic field, configured to move a small camera mounted on a gimbal. It is an absolute positioning device and is run open-loop.

The simplest and most obvious pan-tilt mechanism is the two-stage motor-on-motor (MOM) design. The first motor turns the mechanism through one degree of freedom, usually pan, and the second through the other d.o.f, usually tilt. The second motor must be powerful enough to move the camera sensor. The first must move both the camera and the second motor. The MOM design therefore usually consists of one larger motor and one smaller one. Such a design is inefficient because, as we show, it is not necessary to carry one motor on top of another one. An example of a commercially available MOM design is the pan-tilt actuator shown in (Figure 2).

An alternative to the inefficiencies of the MOM design uses a linkage. We experimented with this approach with the Platform Pantilt, a pan-tilt actuator based on two linear stepper motors (Figure 3).

The Platform Pantilt moves a platform by raising and lowering two shafts with linear stepper motors which along with a third fixed shaft, are attached to the platform, The shafts are fixed to single and double universal joints, as shown in Figure 3. This design is similar in some respects to the six degree

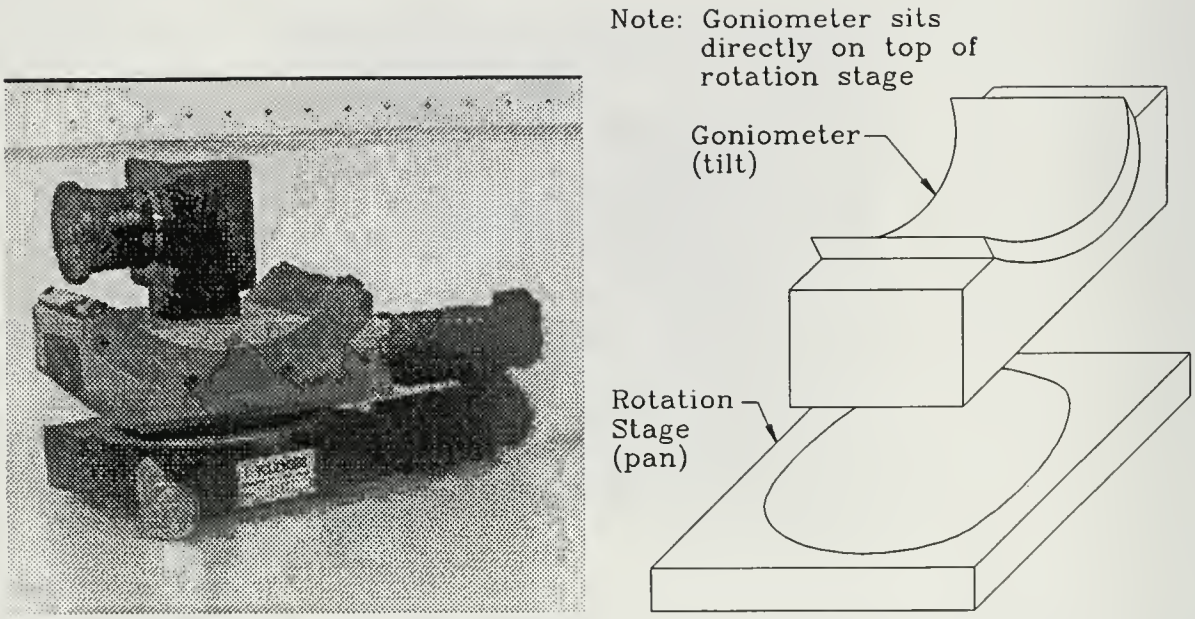

Figure 2: Photo and illustration of a traditional motor-on-motor design. Actuator from Klinger Scientific.

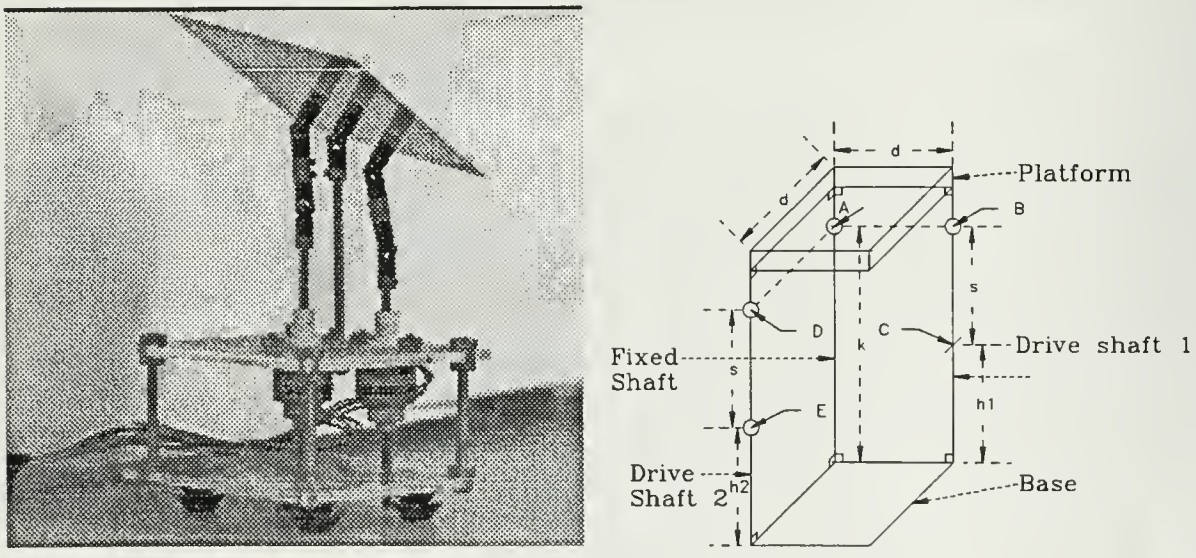

Figure 3: The Platform Pantilt. Photo (**left**). This stepper motor based actuator is capable of positioning a load of 80 grams, for example a small video camera. Illustration (**right**). The three dimensional mechanism we use. Note that circles at points A, B, D and E denote universal joints with two degrees of freedom while the line at point C denotes a pin joint with only one degree of freedom.

of freedom Stewart platform [12,20,21]. The Platform Pantilt is measures 7.5 × 7.5 × 12 cm and can move at rotational velocities of up to 100°/sec. The precision is somewhat limited, however, due to the use of stepper motors, and it is difficult to build this device in a small form factor.

To overcome the limitations of the linkage approach, we implemented the Spherical Pointing Motor (Figure 1), a single direct drive motor with two degrees of freedom. The SPM is capable of panning and tilting a load of 15 grams, for example a CCD image sensor, at rotational velocities of up to 600°/sec. We have also built a miniature camera consisting of a single CCD sensor chip and lens assembly that fits on the rotor of this motor. The complete camera head is 8 × 8 × 10mm and weighs 5 grams. The prototype SPM is 4 × 5 × 6cm and weighs 160 grams. The SPM is part of a space-variant active vision system described in [5,6,22].

2 Background

Pan-tilt mechanisms have been a source of inspiration and frustration to computer vision researchers. The source of inspiration is nature, where humans and animals rely on eye movements to achieve wide field-of-view visual sensing. But the argument from nature is not by itself a compelling reason to build robot eyes that pan and tilt. The alternative to mechanical pan-tilt action is electronic scanning, i.e. computer control of a fixed set of cameras having a combined wide field-of-view. Selective attention can be implemented by a variety of addressing methods, for example the inverted pyramid of Burt [7,8]. Such "software pan-tilt" mechanisms are considerably more convenient and reliable than their motorized counterparts. At present, the relative advantages of software versus hardware based active vision is open: many research groups are pursuing both strategies.

One source of frustration with pan-tilt devices is acquiring or building, then calibrating and controlling the mechanism itself. Until recently, no manufactures have provided devices specifically designed for computer control of robot cameras. Low-speed inexpensive motorized pan-tilt camera platforms are available, for example from Edmund Scientific (catalog number F38,485), but these have no computer controls. Remote control pan-tilt devices intended for security camera applications, for example the Graystone Model V370PT, tend to be too slow (6 degrees per second) and too heavy (16 lbs.) for many robotic applications. Few of these devices have computer controls or position feedback information other than visual. The motion picture industry has also developed computer controlled pan-tilt devices. One example is the Kaleidoscope Hothead II, made by Shepperton Film Studios. Although a digital interface is available, this device is intended to carry a large load such as a 35mm motion picture camera, and although it achieves relatively high speed (140 dps), it is very expensive. Another source of pan-tilt mechanisms is the lighting industry, which applies them to stage lighting, exhibition and advertising. A high-speed computer controlled pan-tilt mechanism for stage lights is available from Multiline, but its bracketing and high cost make it unappealing for robot vision. A number of manufacturers (for example Aerotech, Daedel, Unislide, and Klinger Scientific) make computer controlled mechanisms that can be assembled into pan-tilt devices. Better suited for manufacturing and optics applications, the high resolution of these devices (less than 1 arc minute) makes them overqualified for many computer vision applications and contributes to their high cost and weight.

Perhaps because of their familiarity and availability, if not their generality and programmability, robot arms have often been the choice of vision researchers trying to actuate their cameras. Baloch and Waxman used a 5-axis robot arm mounted on top of a mobile robot as a camera pointing mechanism [4]. Allen also reported mounting a TV camera on a robot arm [3]. Raviv used a cartesian manipulator to implement camera pan, tilt, roll and translation [17].

Finally, a number of researchers including ourselves have embarked on building their own pan-tilt devices from scratch. Krotkov built what is now recognized as the first robot head, a computer controlled

mechanism for moving two cameras [16]. Abbot and Ahuja report an 11 degree of freedom mechanism to control pan, tilt, vergence, horizontal translation, and lens parameters [1,2]. From Osaka University, Kawarabayashi et. al. report building an active vision "head" to control pan, tilt, vergence, zoom and focus parameters of a pair of cameras [14]. The pan-tilt mechanism in all three of these designs is a MOM design. Dickmanns also reports a "fast" two-axis pan-tilt device carrying two cameras, one with a wide-angle view and the other telephoto, mounted atop their robotic automobile [11]. At Harvard, Clark and Ferrier constructed a seven degree-of-freedom "head" to control pan, tilt, and the vergence, focus and aperture of two cameras [10]. At lest one two-eye system, the Rochester Robot, contains independent pan controls for two cameras on a tilting platform, in contrast to other systems in which vergence is coupled [9].

The principal thrust of the present paper is the control of two degrees of freedom (pan-tilt) with a single, direct drive actuator, with sufficient speed and accuracy to provide a basis for light weight and inexpensive active vision systems.

3 Spherical pointing motor theory

The Spherical Pointing Motor (SPM) is an absolute positioning device, designed to orient a small camera sensor in two degrees of rotational freedom. The basic principle is to orient a permanent magnet to the magnetic field induced by three orthogonal motor windings by applying the appropriate ratio of currents to the three coils. A simple way to understand this device follows: The net magnetic field of the three coils may be visualized as defining a vector (dipole) oriented at angles (Θ, Φ) on the unit sphere. The angles (Θ, Φ) are determined by the three coil currents. The rotor dipole then aligns itself with the net coil field to provide the actuation.

We have built two types of SPMs: one having the coils on the inside, free to rotate on a gimbal inside a fixed magnetic field, (Figure 4); the other having the coils on the outside and the magnets attached to the gimbal inside the coils (Figure 5). It is possible to build the smallest possible motor using the external coil design, so that is the approach we focus our attention on.

In this section we look at the transfer function taking input current to pan and tilt angles. We point out some design constraints on the configuration of the coils and the permanent magnets, and show why the external coil design is preferable to the internal one. We discuss calibration of the motor, power dissipation and dynamics.

Both designs are constrained by two principles that affect the range of motion of the motor. The SPM is meant to be used as a pointing device. As such, it has a "home position", defined as the initial resting position from which the motor can make pan or tilt excursions of limited extent. Assuming that we want the home position to be centered within the possible excursions, we are led to the following constraints:

1. The permanent magnets must be positioned so that the field they define is orthogonal to both axes of rotation of the gimbal when it is in home position.

2. The camera must be positioned on the rotor so that its optical axis is orthogonal to both axes of rotation of the gimbal when it is in home position. Note that this is equivalent to being aligned with the magnetic field if the first design constraint is satisfied.

These design principles arise because the motor is limited to two mechanical degrees of freedom and because the motor rotation can not be controlled about an axis aligned with the permanent magnetic field. To understand why this is so, we must examine the electromagnetic principle that provides the torque to move the motor.

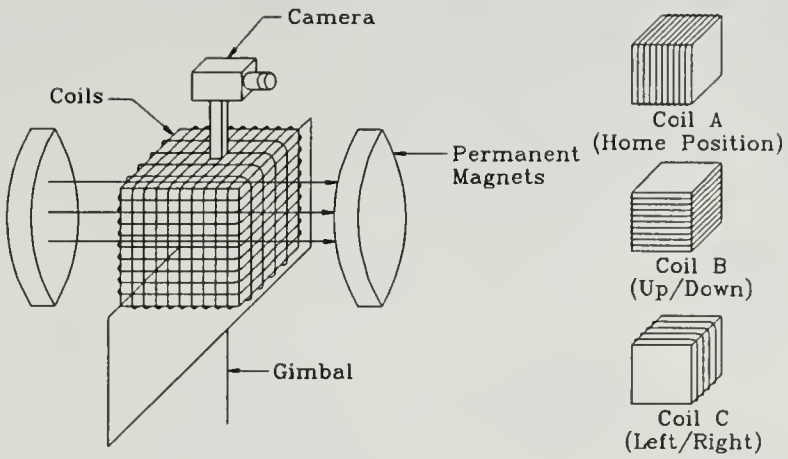

Figure 4: **left)** Illustration of the internal spherical pointing motor shown in its home position. **right)** Labels for the three coils.

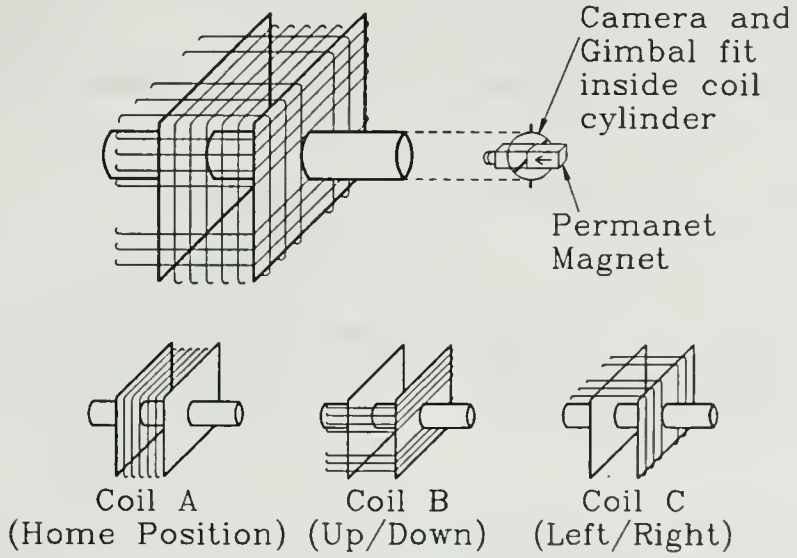

Figure 5: **top)** Illustration of the external spherical pointing motor shown in its home position. **bottom)** Labels for the three coils.

The force on the coils comes from the basic electromagnetic principle that there is always an induced force on a current-carrying wire in a permanent magnetic field. Further, there will be a torque on a current-carrying wire loop in a permanent magnetic field in such a direction that the loop will move to make the normal to the plane of the loop align with the magnetic field. This is shown in Figure 6.

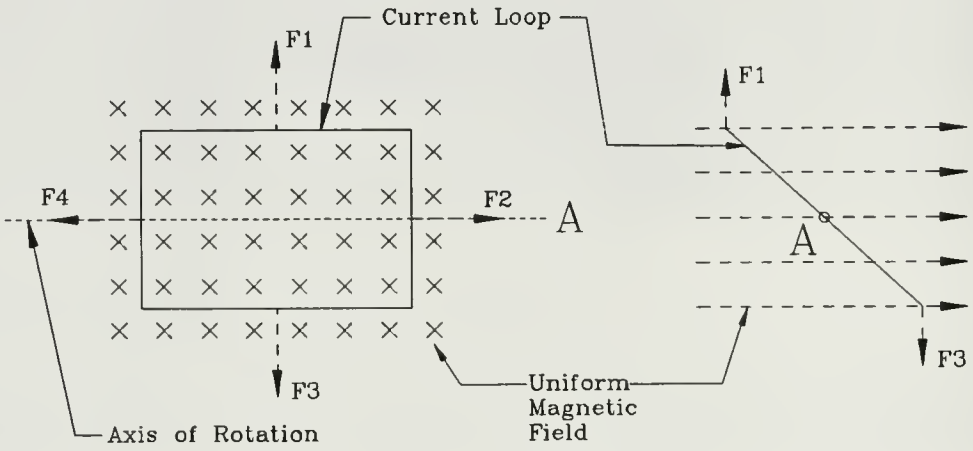

Figure 6: Torque on a current loop. **left)** Coil on horizontal axis with clockwise current. Uniform magnetic field normal to the page. Forces $\mathbf{F_2}$ and $\mathbf{F_4}$ are aligned with the axis and produce no net force. Forces $\mathbf{F_1}$ and $\mathbf{F_3}$ rotate the coil so that the coil encloses as many magnetic field lines as possible which occurs when the normal to the plane of the coil is aligned with the magnetic field. **right)** The same loop, but viewed from the side. (Adapted from [13, P. 541])

Given a coil of wire in a uniform magnetic field $\mathbf{B}$, the torque τ exerted on the coil is the cross product

$$\tau = \mu \times \mathbf{B} \tag{1}$$

where μ is the magnetic dipole moment having direction perpendicular to the coil and magnitude

$$|\mu| = NiA \tag{2}$$

where N is the number of windings in the coil, i is the current in the wire, and A is the area inside each winding [13,15]. The sign of μ is determined by the direction of current in the wire loop. When a nonzero current i flows through the loop, there will be a torque on the loop so that the loop will rotate to its minimum energy configuration where $\tau = 0$, i.e. μ is aligned with $\mathbf{B}$. Note that in the SPM, the permanent magnetic field is not uniform around the area of the coil. This difference is discussed in Section 7.

This shows that the torque is maximum when the angle between μ and $\mathbf{B}$, $\Theta = 90$ and drops to nothing when $\Theta = 0$. When the coil is at position $\Theta = 0$, it is at its minimum potential energy and there is no force on it. Because of this relationship between torque and angle, the friction of the bearings must be minimized. The precision of the motor is inversely related to the amount of friction in the bearings. This is because fine movements of the motor occur at very small angles where the torque is very small, and such fine movements must overcome the friction of the bearings.

We now examine the first design constraint. If this constraint is not satisfied, then it is not possible to both pan and tilt the motor from the home position. Coils A and B control the tilting while coils

A and C control the panning (Figure 4). When the motor has panned 90^0, coil B has kept its original orientation with respect to the magnets, but coils A and C have swapped their relative orientation. This is depicted in Figure 7 for the internal coil motor and the analog for the external coil motor is in Figure 8. This position can be reached by energizing coil C while turning off coils A and B. In this position, the pan angle is controlled, but there is no way to control the tilt angle in this orientation. This is because the tilt axis is aligned with the magnetic field and no torque can be exerted around this axis. This is proved in Section 4. Without the first design constraint, the home position could be as depicted in Figure 7 in which case the motor could not be tilted along the vertical meridian.

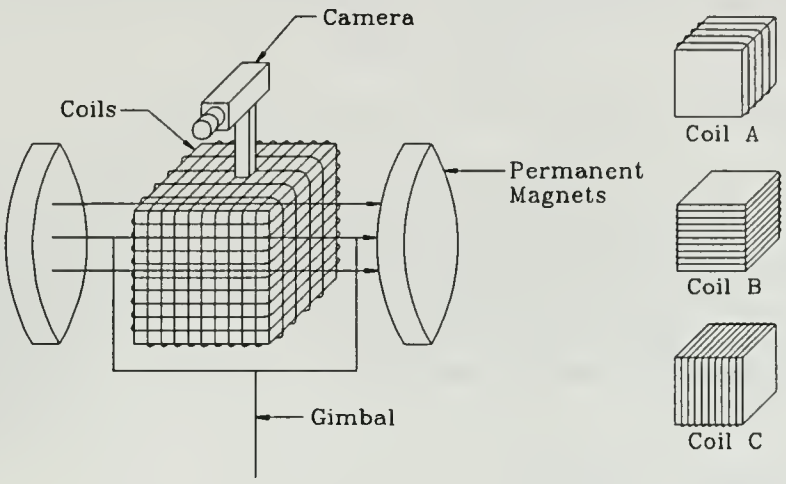

Figure 7: **left)** The internal coil motor panned 90^0 so that tilting is not possible. **right)** The coil labels for the motor in this position. Notice how coils A and C have swapped orientations.

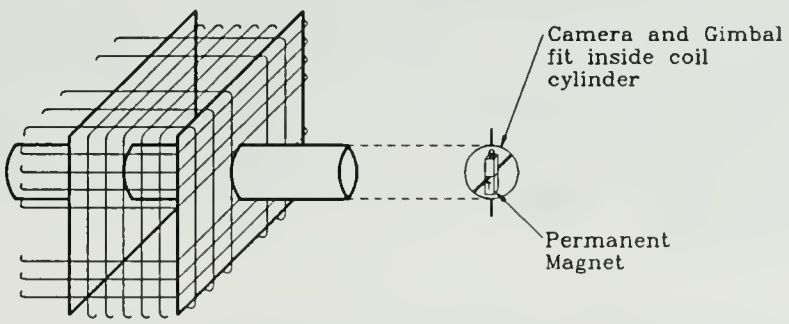

Figure 8: The external coil motor panned 90^0 so that tilting is not possible.

The second design constraint stems from assuming that two degrees of freedom desired for the camera are pan and tilt. If instead roll (rotation about the optical axis) and either pan or tilt is desired, then the second design constraint is not necessary. This constraint comes directly from the mechanical

degrees of freedom available. If pan and tilt are desired, the camera's optical axis must be orthogonal to the two degrees of mechanical freedom.

This has an undesirable affect for the internal coil motor. Because the first design constraint requires that the permanent magnets must also be positioned orthogonally to both axes of rotation, the optical axis of the camera must be aligned with the permanent magnetic field. Since the camera is between the two permanent magnets, its field of view will be obscured by the magnets. Therefore, some method of looking over the magnets must be found. This could possibly be done with mirrors, or as depicted in Figures 5 and 8, the camera could be mounted on a stalk. This gives the external coil motor a clear advantage because the camera is located in the center of the motor. This not only decreases the moment of inertia, but also allows the camera to be rotated around the focal point of the lens which is usually desired for machine vision applications.

4 Theoretical Calculation of motor position

Here we investigate the relation between motor orientation and coil currents. The current in each coil induces a magnetic field normal to the plane of the coil. Because the magnetic fields from the three coils add vectorially, only the ratio of the currents through the coils is important to determine orientation. The motor is an absolute positioning device. This means that applying a set of currents to the coils creates a torque on the rotor that will turn it to the position of lowest potential energy. At this point, there is no torque, and thus no movement. In this section, we assume ideal coils, i.e., they are perfectly symmetrical, have the same number of turns, and are the same size. We deal with the realistic case in Section 5.

4.1 Position given currents

From Equation 1, we know that the torque on a coil is proportional to the sine of the angle between the normal to the coil and the magnetic field. If μ is aligned with $\mathbf{B}$, pointing in either the same or the opposite direction, there is no torque. However, when when they are pointing in the same direction, the potential energy is minimum and the coil is in a stable resting state. If they are pointing in opposite directions, the potential energy is maximum and the coil is in an unstable resting state. If the coil is slightly perturbed, it will swing around 180^0 to reach the minimum potential energy state.

We will use the external coil motor as an example, but the following derivation applies equally to the internal coil motor. Here, we talk about torque on the magnets for the external coil motor, but an equal torque acts on the coils for the internal coil motor. For example, the torque on the magnets due to coil A for the external coil motor is equivalent to the torque on coil A for the internal coil motor.

We will use coil labels shown in Figure 4. As the torque from each coil is dependent on the motor orientation, we must calculate when the sum of the torques on all three coils vanishes. The resting position is determined by

$$\tau_A + \tau_B + \tau_C = 0. \tag{3}$$

We define the coordinate system we will use in Figure 9. Here, both the permanent magnetic field and the home position are defined to lie in the direction of the positive x-axis. Θ (or tilt angle) is defined as the negative rotation about the z-axis and Φ (or pan angle) is defined as the negative rotation about the y-axis.

Let us examine the torque due to coil A. The magnetic field, $\mathbf{B} = (1,\ 0,\ 0)$. When the motor is in home position, coil A has the magnetic dipole moment, $\mu_A = N_A A_A i_A(1,\ 0,\ 0)$. We use here, the

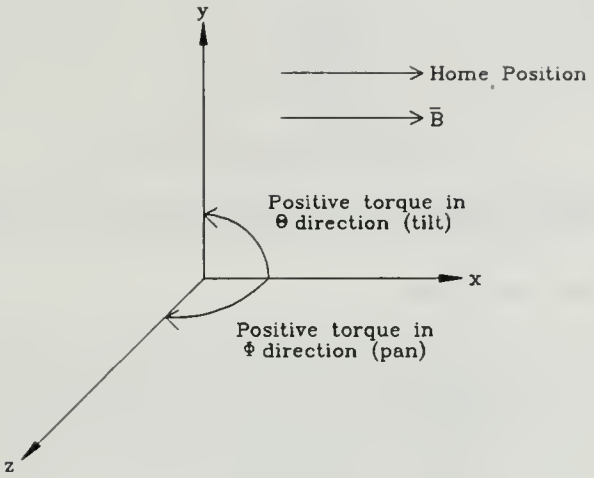

Figure 9: The coordinate system used for calculations. The permanent magnetic field and the home position both lie along and in the direction of the positive x-axis.

constant $K_A = N_A A_A$. To calculate the torque from coil A at position $(\Theta,\ \Phi)$, we rotate μ_A by Θ around the z-axis and then by Φ around the y-axis, yielding the new dipole moment, μ'.

$$\begin{aligned} \mu'_A &= K_A i_A(1,\ 0,\ 0) \cdot [\mathrm{rot}_Z(\Theta)] \cdot [\mathrm{rot}_Y(\Phi)] \\ &= K_A i_A(\cos\Theta\cos\Phi,\ \sin\Theta,\ -\cos\Theta\sin\Phi) \end{aligned}$$

Then,

$$\begin{aligned} \tau_A &= \mu'_A \times \mathbf{B} \\ &= K_A i_A(0,\ -\cos\Theta\sin\Phi,\ -\sin\Theta) \end{aligned}$$

We can calculate the torque from coils B and C similarly.

$$\begin{aligned} \mu'_B &= K_B i_B(0,\ 1,\ 0) \cdot [\mathrm{rot}_Z(\Theta)] \cdot [\mathrm{rot}_Y(\Phi)] \\ &= K_B i_B(-\sin\Theta\cos\Phi,\ \cos\Theta,\ \sin\Theta\sin\Phi) \\ \tau_B &= \mu'_B \times \mathbf{B} \\ &= K_B i_B(0,\ \sin\Theta\sin\Phi,\ -\cos\Theta) \end{aligned}$$

and

$$\begin{aligned} \mu'_C &= K_C i_C(0,\ 0,\ 1) \cdot [\mathrm{rot}_Z(\Theta)] \cdot [\mathrm{rot}_Y(\Phi)] \\ &= K_C i_C(\sin\Phi,\ 0,\ \cos\Phi) \\ \tau_C &= \mu'_C \times \mathbf{B} \\ &= K_C i_C(0,\ \cos\Phi,\ 0) \end{aligned}$$

Finally, we calculate the position using Equation 3.

$$K_A i_A(0,\ -\cos\Theta\sin\Phi,\ -\sin\Theta) + K_B i_B(0,\ \sin\Theta\sin\Phi,\ -\cos\Theta) + K_C i_C(0,\ \cos\Phi,\ 0) = 0$$

This results in the solution

$$\Theta = \tan^{-1}\left(\frac{-K_B i_B}{K_A i_A}\right) \tag{4}$$

$$\Phi = \tan^{-1}\left(\frac{K_C i_C}{K_B i_B \sin\Theta - K_A i_A \cos\Theta}\right) \tag{5}$$

Thus, the position of the motor (Θ, Φ) can be calculated given the currents applied to the three coils.

4.2 Currents given position

Given a desired motor position, we would like to calculate the coil currents necessary to attain that position. As previously stated, because there are three coils and only two mechanical degrees of freedom, the motor position depends upon the ratio of the currents in the coils. Thus, we can fix one of the coil currents, and calculate the other relative currents. Then the scale of the three currents will control the torque with which the motor is moved to the specified position. Note that the three degrees of freedom corresponding to the three coil currents are (Θ, Φ), and magnitude of the torque, τ.

Assume i_A constant. Then from Equations 4 and 5,

$$i_B = \frac{-K_A}{K_B} i_A \tan\Theta \tag{6}$$

$$i_C = \frac{-K_A i_A}{K_C}(\sin\Theta \tan\Theta + \cos\Theta)\tan\Phi \tag{7}$$

The three currents are then scaled so that the largest current magnitude is set to a maximum, i_{max}. That is,

$$\max(|i_A|, |i_B|, |i_C|) = i_{max}$$

Figure 11 shows plots of the calculated currents vs. position for each of the three coils along with the actual currents produced from the calibration procedure described in Section 5.

4.3 Illustration of design constraint

Using these definitions for Θ and Φ, we can now explain the first design constraint more thoroughly: the permanent magnet must be positioned so that the field they define is orthogonal to both axes of rotation of the gimbal when it is in home position. As previously stated, this constraint comes from the fact that when the motor is panned 90^o (i.e., $\Phi = 90^o$), there is no control of the tilt (i.e., Θ is undefined).

Here we show that setting $\Phi = 90^o$ results in Θ being undefined. The case where K_A or K_B or K_C equals 0 represents a motor with one or more coils missing. This is a trivial case, so we assume that $K_A, K_B, K_C > 0$. Now plug $\Phi = 90^o$ into Equation 5

$$\tan^{-1}\left(\frac{K_C i_C}{K_B i_B \sin\Theta - K_A i_A \cos\Theta}\right) = 90^o$$

$$\frac{K_C i_C}{K_B i_B \sin\Theta - K_A i_A \cos\Theta} = \infty$$

This implies that $i_c \neq 0$ and that

$$K_B i_B \sin\Theta - K_A i_A \cos\Theta = 0$$

$$\tan\Theta = \frac{K_A i_A}{K_B i_B}$$

$$\frac{K_A i_A}{K_B i_B} = \frac{-K_B i_B}{K_A i_A}$$

$$(K_A i_A)^2 = -(K_B i_B)^2$$

This is satisfied only when $i_A = i_B = 0$. But by Equation 4, $\tan\Theta$ is defined by $(-K_B i_B)/(K_A i_A)$ which is undefined when $i_A = i_B = 0$. Therefore, when $\Phi = 90^o$, Θ is undefined.

5 Calibration

The calculation of motor position for specified currents would be accurate in the ideal case where all three coils were perfectly symmetrical, had the same number of turns, and were the same size. In general, none of these things are true. Thus the calculated currents gives only an approximation to the actual position of the motor.

The motor must be calibrated to associate motor positions with the related set of currents that moves the motor to these positions. Only a small number of calibration points are necessary (depending on the desired precision of the motor). Points between the calibrated positions can be approximated with linear interpolation.

We have developed a procedure for automatic calibration of the SPM. It is based on image feedback from a camera mounted on the rotor of the motor. It assumes that a calibrated image sensor and lens are used, i.e., that it is known how many degrees each pixel subtends, and that this is constant throughout the field-of-view. The basic idea is that a scene of black dots on a white background is imaged. For each motor position that is to be calibrated, the motor is moved approximately to that position using the calculated currents of Section 4. The image is analyzed, and the position of the relevant dot is used to calculate the actual position of the motor. This position is then associated with the coil currents by creating a look-up-table, calib, that stores the three coil currents for each motor position.

The workspace of the motor is larger than the field of view of the camera, so the scene must consist of more than one dot. To make the calibration procedure as automatic and as easy to use as possible, we do not want to measure the scene externally. Instead, the algorithm should work with only approximate knowledge of the positions of the dots. The only requirement is that there are enough dots so that the entire workspace of the motor is covered, and that it is possible to view the dots in pairs so that the position of one dot can be determined by its position relative to that of a previously determined one. In this way, the position of each dot can be precisely measured automatically by the calibration procedure. The scene used to calibrate the prototype motor is shown in Figure 10.

The algorithm, **calibrate** for calibrating the SPM with a multiple dot scene follows where the algorithms **center_dot**, **find_dot** and **centroid** are described afterwards. It assumes the scene is arranged so that initially, the center dot is approximately centered in the motor workspace, and thus in the camera field of view when the motor is in home position. A data structure is used supplying information about the arrangement of the scene. The algorithms are specified for space-variant images which are briefly summarized in Appendix A. The constants are defined in Appendix B. For each dot

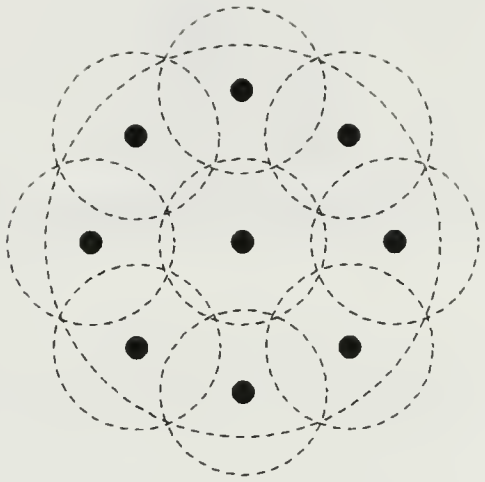

Figure 10: The solid dots comprise the scene used to calibrate the SPM. The nine smaller dashed circles are not part of the calibration pattern, but represent the field of view of the camera when centered on each dot. The single large dashed circle is also not in the scene, but represents the workspace of the motor. The entire workspace of the motor is covered by the small dashed circles.

in the calibration pattern, the data structure contains:

dot_scene table

Variable	Description
motor_init	(Θ, Φ) position of where to initially move the motor for this point. This position should be defined such that the new dot and a previously calibrated dot are both in the field of the view of the camera when the motor is moved to this position.
new_coord	Estimated position of new dot at motor position, motor_init
old_coord	Estimated position of previously calibrated dot at motor position, motor_init
old_id	Index into this data structure to identify which previously calibrated dot is used

In all of these algorithms, the dot is defined as a single connected component whose values are below a threshold which is assumed to have been previously computed. Three routines are called which are not explicitly defined here. soap_bubble uses a standard relaxation technique to fill in the undefined values of the calibration table, calib. median_filter applies a standard 5×5 median filter to calib to eliminate bad points. smooth applies a standard 3×3 smoothing filter to calib to smooth noise.

The prototype SPM has been calibrated using calibrate and the scene depicted in Figure 10. The results are shown in Figure 11 along with the ideal case. The currents for each coil are shown over a workspace of $\pm 30°$ in Θ and Φ.

Algorithm: **calibrate**
Function: This calibrates the SPM, creating a look-up-table associating coil currents for specific motor positions. This is accomplished automatically, imaging a scene with multiple dots. For each position to be calibrated, the motor is moved to that position using the calculated values. The dot is then searched for starting at its estimated position. Its actual position is associated with the motor position and entered in the calibration table.
Input: **dot_scene** table
Output: Calibration table: calib[Θ, Φ] are coil currents for each calibrated motor position.

```
For each calibration point, [k,l], in calib
    calib[k,l] ← undefined
End For
Move motor to (0, 0), i.e., home position
For each dot in the scene, dot_index
    Move motor to motor_init[dot_index]
    Acquire image
                        /* Find absolute position of current dot */
    zero_pt[dot_index] ← find_dot(new_coord[dot_index])
    If not the first dot Then
        old_dot_position ← find_dot(old_coord[dot_index])
        zero_pt[dot_index] ← zero_pt[dot_index] - old_dot_position + zero_pt[old_id[dot_index]]
    End If
    (CenterΘ, CenterΦ) ← center_dot(new_coord[dot_index])
    For each motor position, (Θ, Φ), to be calibrated with the new dot
        Move motor to estimated position, (Θ, Φ), using calculated table
        Acquire image
                        /* Convert motor position to image position */
        estimated_dot_position ← (NROWS/2 - (CenterΘ - Θ)/DEG_PER_PIXEL,
            NCOLS/2 - (CenterΦ - Φ)/DEG_PER_PIXEL)
        new_dot_position ← find_dot(estimated_dot_position)
                        /* Convert new_dot_position to calib indices */
        [k,l] ← DIM_CALIB/2 + (new_dot_position - zero_pt[dot_index]) × DEG_PER_PIXEL ×
            DIM_CALIB / DEG_OF_WORKSPACE
        If calib[k,l] = undefined Then
            calib[k,l] ← -1 × (Motor currents for each coil at this position)
        Else
            calib[k,l] ← (calib[k,l] - (Motor currents for each coil at this position))/2
        End If
    End For
End For
calib ← soap_bubble(calib)
calib ← median_filter(calib)
calib ← smooth(calib)
```

Algorithm: **center_dot**
Function: This moves the motor to center the dot in the image. It is an iterative process, moving the motor to center the dot using the approximate values of the calculated motor position look up table.
Input: Starting motor position, (Θ, Φ)
Estimated dot position, p_1, in logmap image, L
Output: Motor position that results in centered dot.

Do
    Move motor to (Θ, Φ)
    Acquire image
    (dot_row, dot_col) $\leftarrow$ find_dot(p_1)
    $\Theta \leftarrow \Theta$+ (dot_row - NROWS/2) $\times$ DEG_PER_PIXEL
    $\Phi \leftarrow \Phi$+ (dot_col - NCOLS/2) $\times$ DEG_PER_PIXEL
    row $\leftarrow$ NROWS/2
    col $\leftarrow$ NCOLS/2
While dot not centered
return(Θ, Φ)

Algorithm: **find_dot**
Function: This finds the dot in the image starting at the specified location, searching outward. When the dot is found, its centroid is computed and returned.
Input: Starting image location, p_1, in logmap image, L
Output: Centroid of found dot.

For each pixel $p_2 \in L$
    visited[p_2] $\leftarrow$ **FALSE**
End For
visited[p_1] $\leftarrow$ **TRUE**
front $\leftarrow$ 0
back $\leftarrow$ 0
While (($L(p_1) \geq$ threshold) **AND** (front < NPIXELS) **AND** ($a(p_1) > 0$)) **Do**
    For each neighbor $p_2 \in \mathcal{N}(p_1)$
        If (visited[p_2] = **FALSE**) **Then**
            visited[p_2] $\leftarrow$ **TRUE**
            recurse[back] $\leftarrow p_2$
            back $\leftarrow$ back + 1
        End If
        $p_1 \leftarrow$ recurse[front]
        front $\leftarrow$ front + 1
    End For
End While
return(centroid(p_1))

Algorithm: **centroid**
Function: This computes the centroid of a dot in an image given a point in the dot. It assumes the dot is a single connected component of pixels below the threshold. It computes the centroid in the logmap image, but weights the pixels by their area in TV pixels to get the true centroid. It returns the result in TV image coordinates.
Input: Starting image location, p_1, in logmap image L
Output: Centroid of found dot.

If ($a(p_1) = 0$) **Then**
    print("Error: dot searched for at invalid point")
    return(error)
End If
For each point $p_2 \in L$
    visited[p_2] $\leftarrow$ **FALSE**
End For
visited[p_1] $\leftarrow$ **TRUE**
$p_3 \leftarrow 0$
front $\leftarrow$ 0
back $\leftarrow$ 0
total_weight $\leftarrow$ 0
$p_{center} \leftarrow$ (NROWS/2, NCOLS/2)
Do
    For each neighbor $p_2 \in \mathcal{N}(p_1)$
        If ((visited[p_2] = **FALSE**) **AND** ($L(p_2)$ < threshold)) **Then**
            weight $\leftarrow L(p_2) \times a(p_2)$
            $p_3 \leftarrow p_3 +$ weight $\times \mu(p_2)$ /* Convert p_2 to TV coordinates */
            total_weight $\leftarrow$ total_weight + weight
            visited[p_2] $\leftarrow$ **TRUE**
            recurse[back] $\leftarrow p_2$
            back $\leftarrow$ back + 1
        End If
    End For
    $p_1 \leftarrow$ recurse[front]
    front $\leftarrow$ front + 1
While (front $\leq$ back)
If (total_weight > 0) **Then**
    $p_4 = p_3$/total_weight - p_{center}
Else
    $p_4 = (0, 0)$
End If
return(p_4)

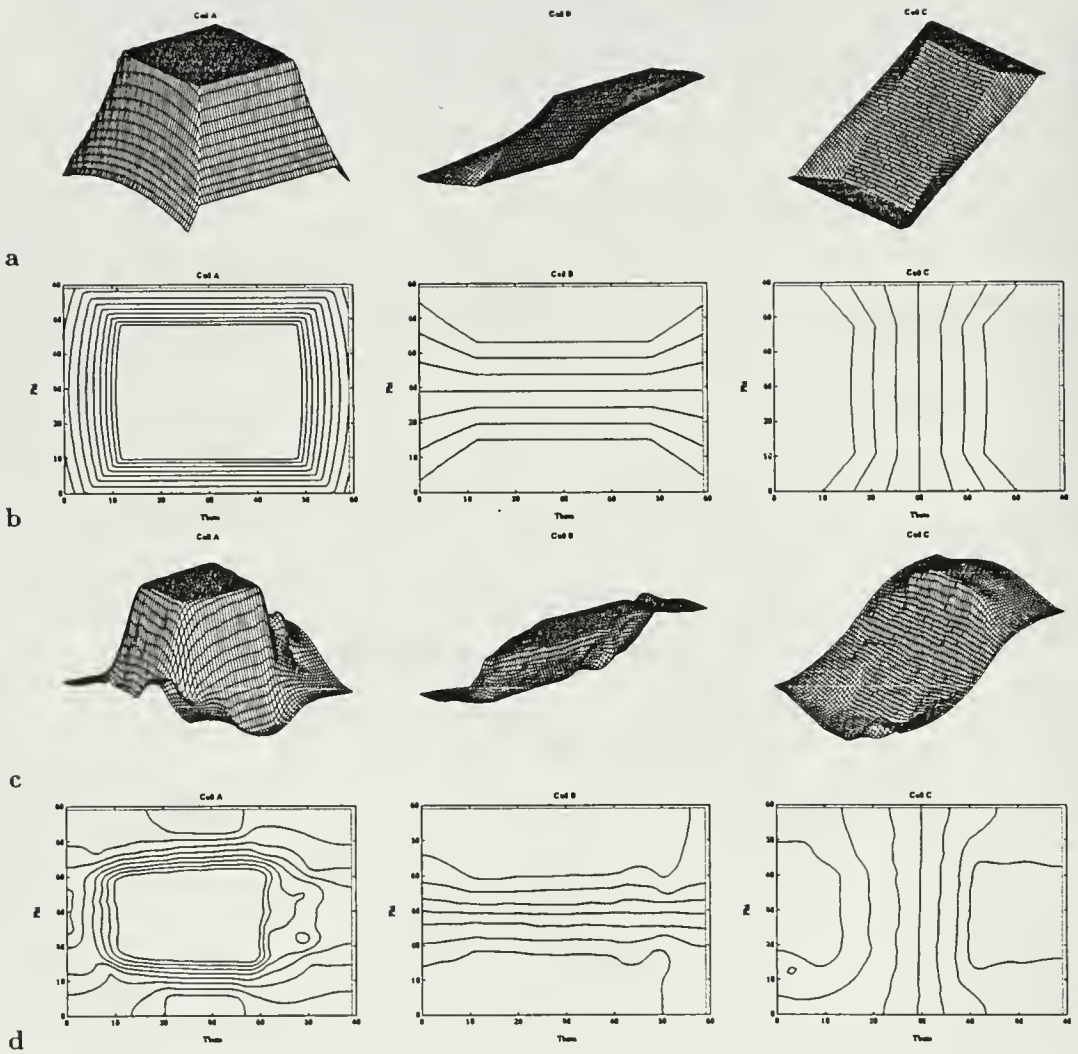

Figure 11: **a)** Theoretical currents vs. position for each of the three coils shown as a mesh plot. **b)** The same as **a)** shown as a contour plot. **c)** Calibrated currents vs. position for each of the three coils shown as a mesh plot. **d)** The same as **c)** shown as a contour plot. The data shown here is for the $\pm 30^{o}$ workspace in (Θ, Φ).

6 Dynamics and control

The dynamics of the spherical pointing motor are that of a simple second order system. When a new set of currents are applied to the coils, a torque is created that moves the rotor to the new position. As calculated in Section 4, this torque is dependent on the angle between the current motor position and the destination position. Let us call this angle Ψ.

The motor will accelerate towards the destination position with the torque decreasing as it is reached. However, it will overshoot and ring around the final position. The ringing is described as follows. The torque $\tau = \kappa \sin \Psi$ for some κ. For small angles, $\sin \Psi \approx \Psi$. Then the position of the motor will follow Equation 8 [13, P. 228].

$$-\kappa\Psi - b\frac{\mathrm{d}\Psi}{\mathrm{dt}} = I\frac{\mathrm{d}^2\Psi}{\mathrm{dt}^2} \tag{8}$$

where b is the damping constant and I is the rotational inertia of the rotor. The approximate solution to this is

$$\Psi = Ae^{-bt/2I}\cos(\omega t + \alpha) \tag{9}$$

where A and α are constants, and the exponential function describes the magnitude envelope of the ringing. The frequency of the ringing is $\omega \approx \sqrt{\kappa/I}$.

The ringing of the SPM was measured by recording the induced voltage of the ringing on a pickup coil of magnet wire that was placed adjacent to the SPM. The recording was made by amplifying the induced voltage and digitizing this through the audio port of a Sun Sparcstation at a sample rate of 8 KHz. Because the SPM is controlled with Pulse-Width Modulation (PWM), the pickup coil not only records the ringing (at approximately 60 Hz), but also records the PWM signal at 1 KHz. The recorded signal is filtered with an FFT to isolate the ringing from the PWM in the induced signal. An example of the ringing shows the result of moving the SPM, uncontrolled, about 20° (Figure 12).

This ringing can be greatly reduced by various open-loop control methods. Perhaps the simplest strategy is to move the move the motor from the initial position to the destination position in small decreasing increments at fixed time intervals. This way, maximum motor velocity is traded off for control. Including the time it takes for ringing to stop, the controlled approach yields a faster average velocity. This method is implemented by moving a fixed percentage of the distance between the current position and final position at each step. This will decrease the motor movement with each step. The motor velocity can then be controlled with either the percentage movement of each step, or the time interval between steps. We use a constant time interval, and vary the percentage movement of each step to experiment with different speeds. We call this the *fixed percentage* control method.

A second slightly more complicated open-loop control strategy based on traditional stepper motor control theory yields better results. The idea, called the *two step* method, is based on the fact that the SPM rotor oscillates with an approximately constant period. We first step the motor to a point midway between the initial and destination positions. This midpoint is determined from the calibration results of Section 5. We then wait for the ringing velocity to be zero at which point we apply a second step to hold the rotor at this position of zero velocity. The energy of the ringing will be largely dissipated, and the rotor will be at the destination position. Although, we don't know exactly when to apply the second step, we can estimate it by waiting half the period of oscillation. This assumes that the period of oscillation is constant, which is not true, but is a close approximation. In practice, because neither the midpoint nor the time at which the currents are changed are exactly correct, not all of the ringing energy is dissipated, and a little ringing of the same period remains, but with vastly reduced amplitude. This approach is unusual in that it takes a constant time to move any distance, where the time is half the period of oscillation. A sample result of this approach is shown in Figure 13.

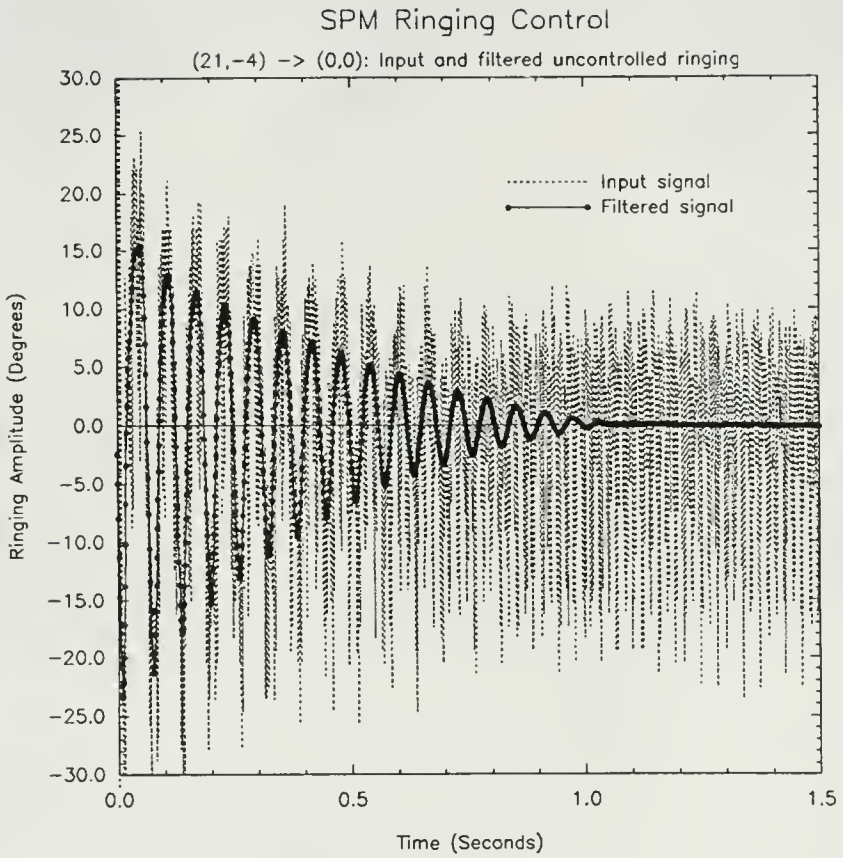

Figure 12: Uncontrolled ringing measurement taken by induced voltage on a separate pickup coil. The input signal (combination of ringing and PWM) is shown along with the filtered signal which isolates the ringing.

We compensated for the imprecision of this strategy by various combinations of the previous two control strategies. The first approach is to apply the two-step method twice, first moving to the midpoint, and then to the destination pont. This method theoretically also takes a constant time, which is twice as long as the single two-step method. We call this approach the *dual two-step* method.

A final variation, called the *multi two-step* method, is to apply the two-step method multiple times with logarithmically decreasing steps. The motor is always moved half way between its current position and the destination position with the two-step method. This takes time $O(\log(\Psi))$ where Ψ is the total angular distance.

Results from these open-loop control strategies are presented in Section 9.2.

One of the motivating factors behind the development of the SPM was to make a motor that could be run by an open-loop controller, and we have accomplished this task. However, if higher performance is needed, a velocity or position sensor could be added to run the motor with a closed-loop control strategy. This would allow the two-step control strategy to applied more accurately, as the zero-velocity point would be known exactly. Not only would this increase the speed of the motor, but it would also increase its accuracy. The motor's supply currents could be 90^o out of phase with the position, like in traditional DC motors. This would result in always driving the motor at its maximum torque and thus the torque would no longer be dependent on the difference between the current and destination position. No closed-loop control strategies have been implemented yet.

7 Design Issues

We want to design the SPM to maximize its torque while minimizing its size and power usage. There are several parameters that we have control over in this design. The diameter of the wire and the area, number of turns, and voltage across the coil as well as the magnetic return path are the parameters that most affect the design, and are the ones that we will discuss here.

The first issue is the magnetic return path. Our magnetic circuit consists of a permanent magnet which generates magnetic field lines with a geometry dependent on the type of material in its immediate vicinity. Magnetic circuits are analogous to electric circuits in that while in electric circuits, different materials have different resistances and the current will follow the path of least resistance, in magnetic circuits, different materials have different permeability and the magnetic field will follow the path of greatest permeability. Because there is only torque on a current loop if the magnetic field goes through the loop and returns outside the loop, it is critical that the geometry of the motor is designed so that the permanent magnetic field lines return outside the coil. Air has very low permeability while iron has very high permeability. By adding an iron return path outside the motor, the magnetic field lines will follow the path of highest permeability, resulting in more magnetic field lines enclosing the coil, and thus more torque. A simulation of the magnetic circuit for the external coil SPM with and without an iron return path is shown in Figure 14. This geometry complicates the calculation of the torque as the magnetic field is not uniform, so in Equation 2, we must use the average magnetic field. We can determine the average magnetic field with magnetic circuit simulation programs, and we can say generally that it is some monotonic decreasing function of the area of the coil.

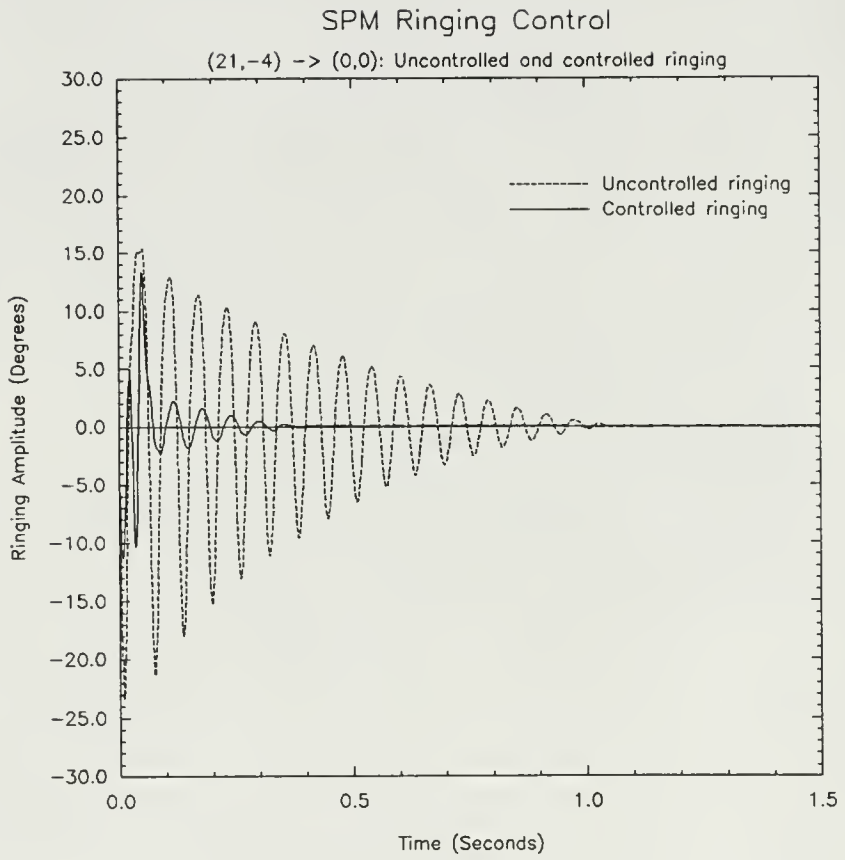

Figure 13: Measurement of two-step open-loop control strategy to reduce SPM ringing. Results are shown for the same movement of 21.4° with and without control. The motor currents are changed to hold the motor at the final position when the motor is expected to have zero velocity. Because the midpoint and timing are not exactly correct, the ringing is not completely elimiated.

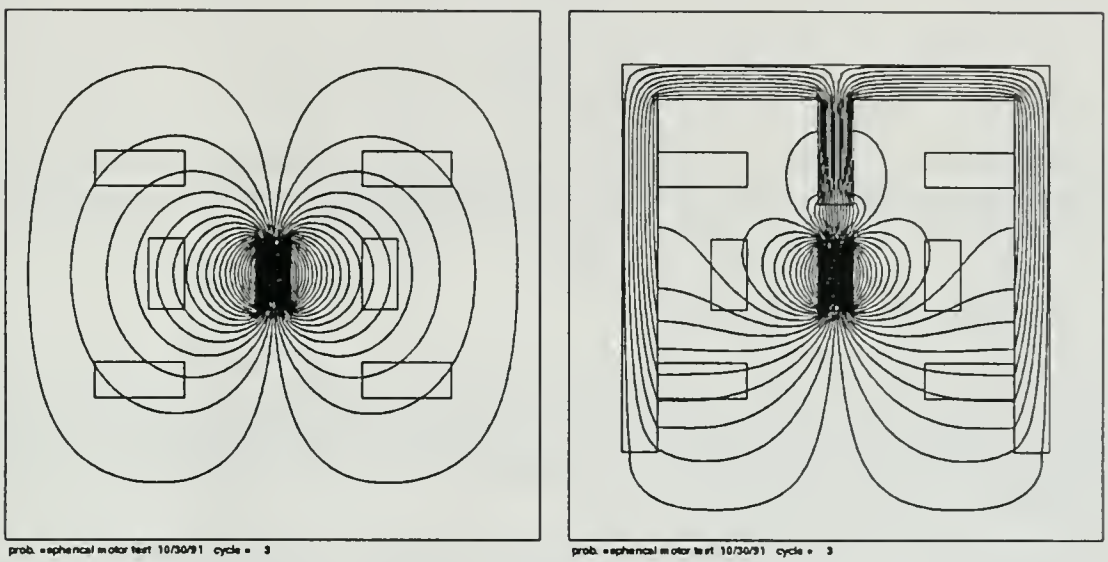

Figure 14: Simulation of magnetic circuit for the SPM **left)** without and **right)** with an iron magnetic return path. The permanent magnet is in the center. A camera mounted on the magnet would be looking towards the bottom of the page. The rectangles represent the coils of the motor. It can be seen that without the magnetic return, only a small percentage of the magenetic field returns outside the coils, but with the magnetic return, an effiency of nearly 50% is achieved.

Now let us investigate the parameters of voltage (V), the number of turn of the coil (N), the area of the coil (A), and the diameter of the wire (D). We know that $\tau \propto NiAB$, and power, $P = Vi$. We want to maximize the ratio τ/P while maintaining a minimum acceptable torque and maximum acceptable power. The resistance of the wire is proportional to the number of turns of the coil, the area of the coil, and inversely proportional to the square of the diameter of the wire, so we can write

$$R \propto \frac{NA}{D^2}$$

Because $i = V/R$, we can rewrite the equation for current as $i \propto (VD^2)/(NA)$. Finally we can rewrite the equations for torque, power and their ratio using only the input parameters:

$$\tau \propto VD^2 \cdot B \tag{10}$$

$$P \propto VD^2 \cdot \frac{V}{NA} \tag{11}$$

$$\frac{\tau}{P} \propto \frac{BNA}{V} \tag{12}$$

From these relationships, we can see that we want to maximize B and N while minimizing V. In doing so, we must also maintain our torque and power requirements and adjust V, D, and A accordingly. The values of these parameters for our prototype SPM are described in Section 9.

8 Controller description

The SPM is controlled by limiting the amount of current in each coil. This can be done either by regulating the voltage on the coils, by using a constant voltage with a Pulse-Width Modulation (PWM) technique, or by using a variable current source. The PWM method is preferred for ease of use, although the variable current source technique has the advantage that the currents, and thus the motor position, are independent of the temperature of the motor.

The SPM controller we use is based on a Motorola M68332 microcontroller which is capable of creating PWM signals. A Unitrode L293N power driver supplies the current for the motor. PWM means driving the motor with a square wave of constant amplitude and period with a variable duty cycle. The percentage of the period where the supply is high is called the duty cycle. A duty cycle of 0 gives no current to the motor while a duty cycle of 100 gives maximum current. The inertia and inductance of the coil effectively smooths the PWM supply.

The polarity of the voltage on the coil also needs to be controlled in order to position the motor everywhere on the unit sphere. Without changing the polarity, only one octant of space would be accessible.

9 Prototype spherical pointing motor

The prototype SPM (Figure 1) is $4 \times 5 \times 6$ cm, weighs 160 grams and is capable of actuating a 15 gram load. Its total workspace is approximately 60^o in both the pan and tilt directions. The permanent magnetic field is estimated at 1 Tesla with an efficiency of about 5%. The number of turns in the coil is estimated. The maximum torque is computed here, where $\Theta = 90^o$. This table shows the parameters of the motor along with its calculated torque and power usage.

Coil	Parameter	Value
Inside	N	630
	D	30 gauge (= .000254 m)
	A	0.000730 m^2
	V	15 Volts
	R	21Ω
	τ	.016N · m or 2.3oz · in
	P	11 Watts
Middle	N	500
	D	30 gauge
	A	0.000993 m^2
	V	15 Volts
	R	26.0Ω
	τ	.014N · m or 2.0oz · in
	P	9 Watts
Outside	N	420
	D	30 gauge
	A	0.00130 m^2
	V	15 Volts
	R	22Ω
	τ	.019N · m or 2.6oz · in
	P	10 Watts

9.1 Accuracy and precision measurements

The precision and accuracy of the SPM were measured by reflecting a laser diode off a reflective surface attached to the rotor. The reflected beam's movement is measured on a wall several feet away as described below.

The precision of the motor is defined as the angular distance between adjacent positions. If the controller consisted of an analog variable current source, the motor's precision would be infinite. As we are using a digital PWM controller, the precision with which we can control the motor is limited by the step size of the PWM duty cycle. The step size is dependent on the frequency of the PWM. Lower frequencies have more precise control of the step. However, lower frequencies also introduce a choppiness which vibrate the motor. We use a 1KHz frequency and are able to specify 4,000 steps in the duty cycle (i.e., 4,000 different duty cycles). As the duty cycle of the PWM on a single coil with a specified polarity changes between 0 and 100, the motor will turn at most 45°. Thus, we can position the motor to steps no smaller than $45°/4000 = 0.011°$ or 0.68 minutes of arc.

The accuracy of the motor is defined as the repeatability of the motor. If the motor were balanced so that gravity was not a factor, then its accuracy would be dependent only upon the friction of the bearings. As there is no iron core, there is no hysteresis. Because the motor, in fact, is not perfectly balanced, the motor position is not constant at different orientations to gravity, but at a fixed orientation, the accuracy is dependent only upon the friction of the bearings.

We measured the motor's accuracy with a laser setup (Figure 15) and found the motor to be accurate to .15°. The camera mounted in our motor returns 192 × 165 pixels with a 33.6° horizontal field of view. This is equivalent to .175° per pixel. For our camera and lens, the SPM is thus accurate to about one pixel.

The procedure for measuring motor accuracy is as follows. The motor is set at a fixed position with the rotor positioned at the place to be measured. The laser is then oriented so that the reflected beam hits the wall at a right angle. This point on the wall is recorded. The motor rotor is moved away and then back to the original position. The distance between the new reflected laser position and the original position is measured, and the accuracy of the motor is calculated according to Equation 13.

The measurement setup is illustrated in Figure 15. Here, l is the distance from the motor to the wall. d is the distance between the first and second laser position on the wall. Φ is the angular difference between the first and second motor positions. The solid lines represent the first motor position, and the dashed lines represent the second. The relation between the laser point movement and the accuracy of the motor is

$$d = l \tan 2\Phi \tag{13}$$

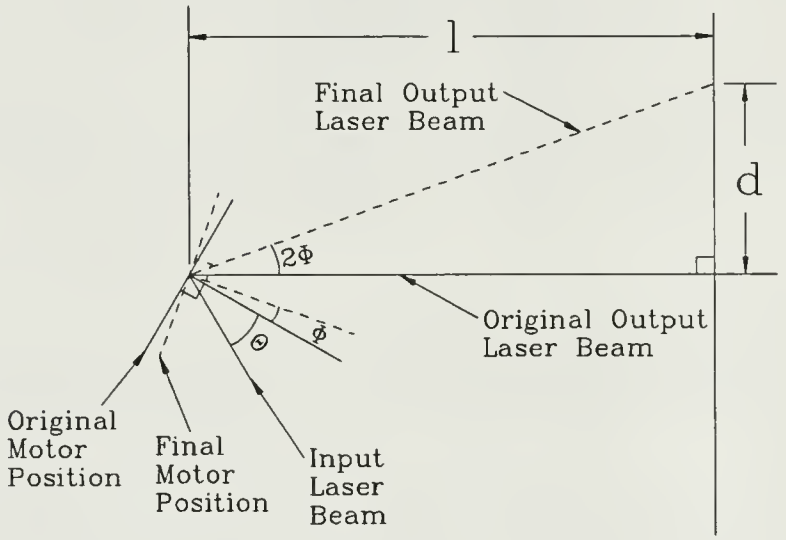

Figure 15: Illustration of our experimental setup for measuring motor accuracy. The laser beam is reflected off the rotor onto a flat surface. The motor is then moved to a new position and back to the original position. The new laser beam position is compared with the original position to see how accurately the motor returned to the original position.

9.2 Velocity measurements

We measured the average velocity of the motor for point to point motions, since we have no ability to measure instantaneous velocity. We recorded the velocity using the technique described in Section 6 for measuring the ringing. The motor controller was programmed to accept motion commands with a specified control strategy over an RS-232 serial port. A program running on a Sun Sparcstation controlled the SPM and automatically recorded and analyzed the results. For each control strategy, ten measurements were made at each of ten different angular movements. The averaged results with error bars showing the variance of each experiment are shown in Figures 16, 17, and 18.

A summary of the control strategies measured follow:

No control Base line for comparing control strategies.

Fixed percentage The motor is moved a fixed percentage of the distance between its current position and the destination position with a fixed delay between each movement.

By making the percentage of movement per step small enough, the ringing can be completely eliminated at the price of velocity. Results shown here are for a percentage selected such that a small amount of uncontrolled ringing remained at the end of the motion.

Two-step The motor is moved to the midpoint between the initial and destination positions. After a delay equal to half the period of the natural motor oscillation, the motor is moved to the destination position.

The midpoint and delay used are an approximation to the ideal values. These result in very good results with a fixed time to move any distance, and a small amount of ringing at the end of the movement. The ringing at the end of the motion does not depend on the amplitude of the motor movement. Rather, it depends on the inaccuracy of the midpoint and delay calculations. A calibrated look-up-table approach would be necessary to eliminate the ringing completely.

Dual two-step The two-step method is used to move first to the midpoint, and then to the endpoint.

This theoretically takes twice as long as the single two-step method, but actually results in slightly better results.

Multiple two-step The two-step method is used multiple times, always moving halfway between the current position and the destination position.

This theoretically takes time $O(\log(\Phi))$ where Φ is the angular distance between the initial and destination positions. Practically, it produced very similar results to the dual two-step method.

Our measuring apparatus was fairly noisy, resulting in the high variance reported. It is clear that all four control strategies provided substantial improvement over the uncontrolled performance. Of these, the two-step methods are a little better than the fixed percentage approach. Because of the noise in our measurements, it is not clear which two-step method is the best.

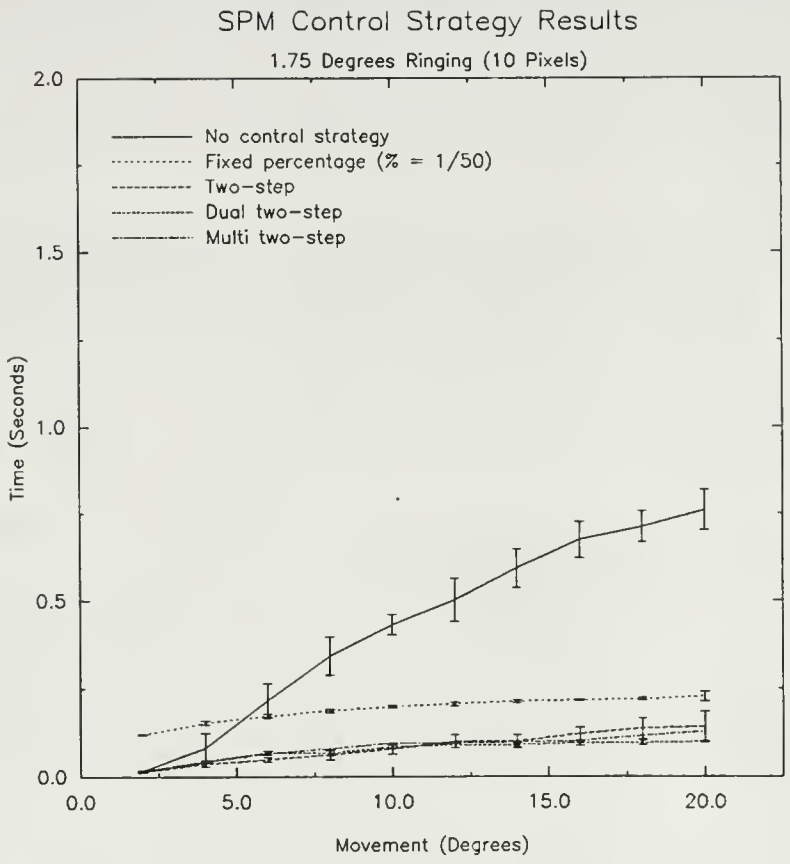

Figure 16: Results of different open-loop control strategies to reduce the ringing of the SPM. Times reported are those after which amplitude of the ringing has been reduced to 1.75° (10 pixels in our camera). Control strategies are discussed in the text.

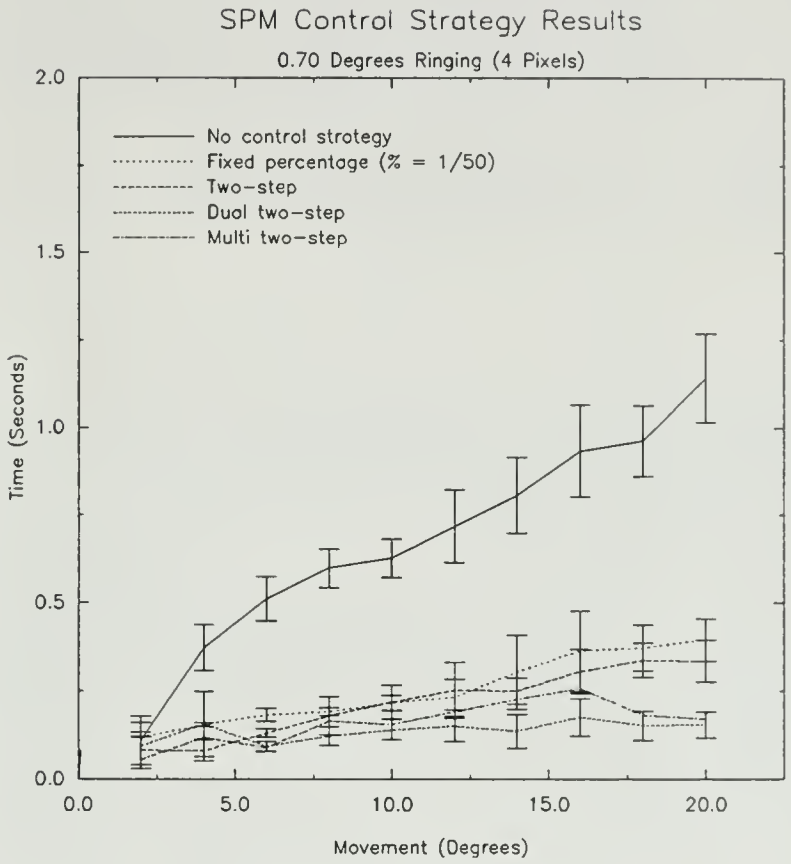

Figure 17: Results of different open-loop control strategies to reduce the ringing of the SPM. Times reported are those after which amplitude of the ringing has been reduced to 0.70° (4 pixels in our camera).

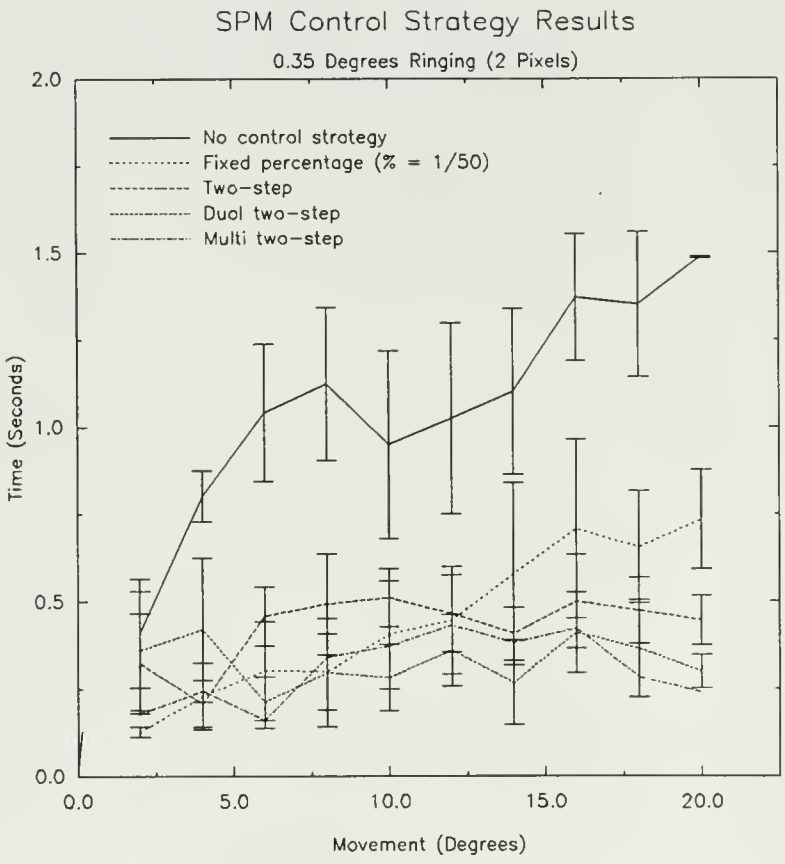

Figure 18: Results of different open-loop control strategies to reduce the ringing of the SPM. Times reported are those after which amplitude of the ringing has been reduced to 0.35° (2 pixels in our camera).

The results are summarized in the following table. For each control strategy, the time to move 2 degrees and to move 20 degrees are given for each of three ringing requirements. The times are specified in milliseconds.

Ctrl Method	2° ringing	4° ringing	10° ringing
No control	408/1480	110/1140	18/760
Fixed percentage	127/734	120/395	120/227
Two-step	332/445	83/334	16/143
Dual two-step	359/298	96/155	18/100
Multi two-step	179/240	56/171	17/128

It should be stressed that the results from these two-step open-loop control strategies were obtained with approximate calculated values for the mid-point and timing values. We fully expect that with a calibrated look-up-table approach, as with the position calibration of Section 5, we will obtain substantially better results.

10 Conclusion

We have developed a new miniature pan-tilt actuator suitable for pointing a camera[1]. The Spherical Pointing Motor (SPM) is comparable in capabilities, yet at least an order of magnitude less in size and cost, than other pan-tilt actuators in common use. It is easy to use since it is an absolute positioning device and is run open-loop. A set of currents applied to the coils moves the motor and holds it at a fixed position. Consisting of wire wound around a metal form, a simple gimbal, and a small rare-earth magnet, the SPM is arguably the smallest and least expensive possible device capable of pointing a camera accurately and at high speed.

In this paper, we described the theory, design and use of the SPM. It is shown that the SPM must be designed with the permanent magnets and the optical axis of the camera positioned in a particular orientation with respect to the gimbal. A discussion of the electromagnetic theory of the SPM shows that the accuracy of the motor is dependent on the friction of the bearings, and thus the mechanical design of the SPM is very important. Equations relating the theoretical coil currents to the motor position are derived. These are then used to calibrate the motor to find the precise relation between coil currents and motor position. The dynamics of the motor are then explored and several open-loop control strategies are examined. Finally, we give results measuring the motor accuracy and velocity.

The SPM currently has good enough operating characteristics to be used in active computer vision systems. We expect to improve its capabilities to move at greater speeds with more precision, and to handle larger loads, such as miniature commercial CCD cameras, by calibrating the control strategies and/or adding feedback for closed-loop operation.

[1]Patent application #07/731,639, entitled "Spherical Pointing Motor" was submitted to the U.S. Patent office in 1991.

A Space-variant images

A space-variant image sensor is characterized by a non-constant pixel size. We have experimented with several sensor designs, the common features of which are large scale changes between the smallest and largest pixels, wide field of view, and a pixel population far smaller than that of a conventional matrix image sensor. One such space-variant sensor is the *logmap* [18,19], in which the pixel pattern approximates the sensor geometry of the human eye.

We often want to display a logmap on a TV screen, or to compute one from a TV picture. Thus we can formally define the logmap as a mapping from a TV image $I(i,j)$ where $i \in \{0,\ldots,NROWS-1\}$ and $j \in \{0,\ldots,NCOLS-1\}$. Let $L(u,v)$ be the logmap, with $u \in \{0,...,NSPOKES-1\}$ and $v \in \{0,...,NRINGS-1\}$.

The forward mapping from TV image space to logmap space is specified by two lookup tables $R(i,j)$ and $S(i,j)$ (Figure 19) where again $i \in \{0,\ldots,NROWS-1\}$ and $j \in \{0,\ldots,NCOLS-1\}$. The forward map is also shown with the correspondence between inverse and forward map pixels. Let $a(u,v)$ be the area (in TV pixels) of a logmap pixel (u,v).

$$a(u,v) = \sum_{i,j} 1 \mid S(i,j) = u \text{ and } R(i,j) = v. \tag{14}$$

The space-variant image is defined by

$$L(u,v) = \frac{1}{a(u,v)} \sum_{i,j} I(i,j) \mid S(i,j) = u \text{ and } R(i,j) = v. \tag{15}$$

The inverse map, illustrated in Figure 20b, is

$$L^{-1}(i,j) = L(S(i,j), R(i,j)). \tag{16}$$

The relationship between a space-variant image and the lookup tables $R(i,j)$ and $S(i,j)$ is illustrated by comparing Figure 19 with Figure 20. The values in the lookup tables depict the row and column addresses of pixels in the space-variant image array. We observe that if n is the number pixels for which $a(u,v) > 0$, then $n \leq NSPOKES \times NRINGS$, and we define $NPIXELS = n$.

The pixel centroid $\mu(p)$ is given by

$$\mu(p) = \frac{1}{a(p)} \sum_{i,j} (i,j)^T \mid S(i,j) = u(p) \text{ and } R(i,j) = v(p). \tag{17}$$

We denote the set of neighbors of a pixel p to be $\mathcal{N}$(p).

Space-variant images along with our miniature system are described in more detail in [5,6,22].

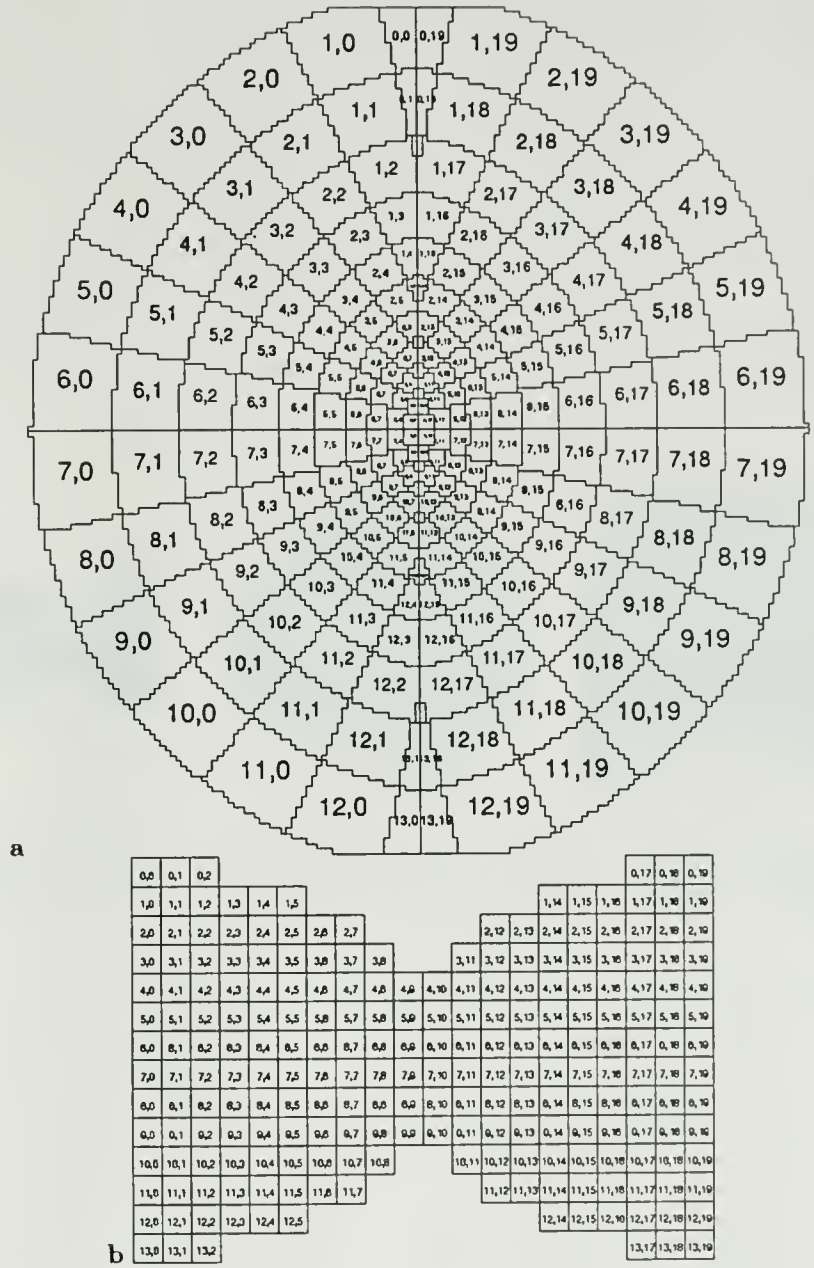

Figure 19: a) The lookup tables $S(i,j)$ and $R(i,j)$ combined into one figure. b) The forward map space.

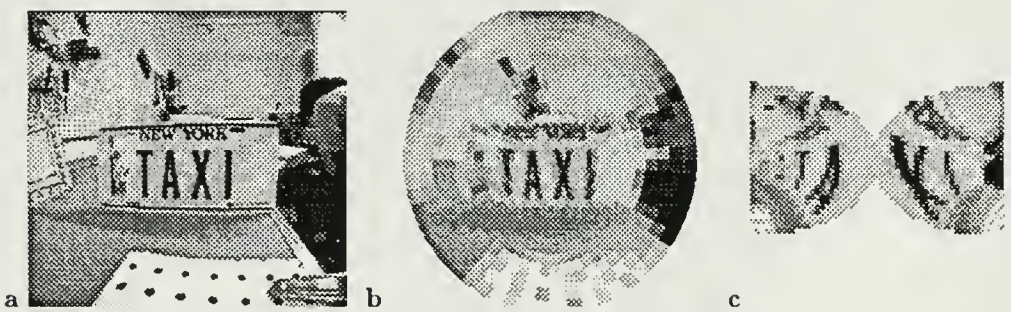

Figure 20: A sample of **a)** an original TV image, $I(i,j)$, **b)** The inverse logmap image $L^{-1}(i,j)$, and **c)** The forward logmap image $L(u,v)$.

B Constant List

$NROWS$	Number of rows in a TV image, $I(i,j)$, i.e., $i \in \{0,\ldots,NROWS-1\}$
$NCOLS$	Number of columns in a TV image, $I(i,j)$, i.e., $j \in \{0,\ldots,NCOLS-1\}$
$NSPOKES$	Number of rows in a logmap image, $L(u,v)$, i.e., $u \in \{0,\ldots,NSPOKES-1\}$
$NRINGS$	Number of columns in a logmap image, $L(u,v)$, i.e., $v \in \{0,\ldots,NRINGS-1\}$
$NPIXELS$	Total number of pixels in a logmap image, $L(u,v)$ which map to TV pixels, i.e, the count of pixels, (u,v) such that $a(u,v) > 0$
DIM_CALIB	Number of calibration points per axis for the SPM
$DEG_OF_WORKSPACE$	Size of workspace of SPM in degrees
DEG_PER_PIXEL	Number of degrees that each pixel subtends for our image sensor and lens combination

References

[1] A. Lynn Abbott and Narendra Ahuja.
Surface reconstruction by dynamic integration of focus, camera vergence, and stereo.
International Conference on Computer Vision, 1988.

[2] A. Lynn Abbott and Narendra Ahuja.
Active surface reconstruction by integrating focus, vergence, stereo, and camera calibration.
International Conference on Computer Vision, 1990.

[3] Peter K. Allen, Billibon Yoshimi, and Aleksandar Timcenko.
Real-time visual servoing.
In *Proceedings of the 1991 IEEE International Conf. on Robotcs and Automation*, pages 851–856, April 1991.

[4] Aijaz A. Baloch and Allen M. Waxman.
Behavioral conditioning of the mobile robot mavin.
Prentice Hall, New Jersey, 1991.

[5] Benjamin B. Bederson.
A miniature space-variant active vision system.
PhD thesis, GSAS, New York University, 1992, expected.

[6] Benjamin B. Bederson, Richard S. Wallace, and Eric L. Schwartz.
A miniaturized active vision system.
In *11th International Conference on Pattern Recognition*, 1992.

[7] Peter J. Burt.
Algorithms and architectures for smart sensing.
IEEE Transactions on Pattern Analysis and Machine Intelligence, pages 139–153.

[8] Peter. J. Burt.
Attention mechanisms for vision in a dynamic world.
9th IEEE Intl. Conf. on Pattern Recognition, pages 977–987, 1988.

[9] ed. C. Brown.
The rochester robot.
Technical Report 257, University of Rochester, 1988.

[10] J. J. Clark and N. J. Ferrier.
Modal control of an attentive vision system.
Second Intl. Conf. Computer Vision, page 514, 1988.

[11] E. D. Dickmanns and V. Graefe.
Applications of dynamic monocular machine vision.
Machine Vision and Applications, 1:241–261, 1988.

[12] E. F. Fichter.
A stewart platform-based manipulator: General theory and practical construction.
The International Journal of Robotics Research, 5(2):157–182, 1986.

[13] David Halliday and Robert Resnick.
Fundamentals of Physics, Second Edition, Extended Version.
John Wiley & Sons, New York, 1981.

[14] Hideharu Kawarabayashi, Makoto Watanabe, Yoshiaki Shirai, Minoru Asade, and Jun Miura.
Tracking of a moving object using an active vision system.

Japan Mechanical Society, Robotics Mechatronics Conference Proceedings, pages 207–212, June 1991.

[15] T. Kenjo and S. Nagemori.
Permanent-Magnet and Brushless DC Motors.
Oxford Scence Publications, 1985.

[16] E. Krotkov, F. Fuma, and J. Summers.
An agile stereo camera system for flexible image acquisition.
IEEE J. Robotics and Automation, 4:108–113, 1988.

[17] Daniel Raviv and Avraham Shapira.
Miniature vision-based flight simulator.
In *4th Annual Conference on Recent Advances in Robotics*, pages 81–86, 1991.

[18] A. S. Rojer and E. L. Schwartz.
Design considerations for a space-variant visual sensor with complex-logarithmic geometry.
10th International Conference on Pattern Recognition, Vol. 2, pages 278–285, 1990.

[19] Alan S. Rojer.
Space-variant computer vision with a complex-logarithmic sensor geometry.
PhD thesis, GSAS, New York University, 1989.

[20] N. Stelman.
Design and control of a six-degree-of-freedom platform with variable admitance.
Master's thesis, Massachusetts Institute of Technology, Dept. of Mechanical Engineering, 1988.

[21] D. Stewart.
A platform with six degrees of freedom.
Proceedings of the Institution of Mechanical Engineers, 1965.

[22] Richard S. Wallace, Ping-Wen Ong, Benjamin B. Bederson, and Eric L. Schwartz.
Space-variant image processing.
Technical Report 589, New York University, Computer Science, Robotics Research, 1991.

This book may be kept

FOURTEEN DAYS

A fine will be charged for each day the book is kept overtime.

GAYLORD 142

PRINTED IN U S A

NYU COMPSCI TR-601
Bederson, Benjamin C.1
A miniature pan-tilt
actuator: the spherical
pointing motor.

NYU COMPSCI TR-601
Bederson, Benjamin C.1
A miniature pan-tilt
actuator: the spherical
pointing motor.

DATE DUE	BORROWER'S NAME

LIBRARY
N.Y.U. Courant Institute of
Mathematical Sciences
251 Mercer St.
New York, N. Y. 10012